

Non-unitary enhanced transfer efficiency in quantum walk search on complex networks

Ugo Nzongani,^{1,2,*} Andrea Simonetto,^{2,†} and Giuseppe Di Molfetta^{1,‡}

¹*Aix-Marseille Université, Université de Toulon, CNRS, LIS, 13288 Marseille, France*

²*Unité de Mathématiques Appliquées, ENSTA Paris, Institut Polytechnique de Paris, 91120 Palaiseau, France*

The task of finding an element in an unstructured database is known as spatial search and can be expressed as a quantum walk evolution on a graph. In this article, we modify the usual search problem by adding an extra trapping vertex to the graph, which is only connected to the target element. We study the transfer efficiency of the walker to a trapping site, using the search problem as a case study. Thus, our model offers no computational advantage for the search problem, but focuses on information transport in an open environment with a search Hamiltonian. The walker evolution is a mix between classical and quantum walk search dynamics. The balance between unitary and non-unitary dynamics is tuned with a parameter, and we numerically show that depending on the graph topology and the connectivity of the target element, this hybrid approach can outperform a purely classical or quantum evolution for reaching the trapping site. We show that this behavior is only observed in the presence of an extra trapping site, and that depending on the topology, the increase of non-unitary operations can be compensated by increasing the strength of the quantum walk exploration. This compensation comes at the cost of reducing or even suppressing the searching feature of the evolution. In that case, the unitary dynamics will only induce a regular quantum walk behavior. We also relate the optimal hybrid regime to the entropy's decay rate. As the introduction of non-unitary operations may be considered as noise, we interpret this phenomena as a noisy-assisted quantum evolution.

I. INTRODUCTION

Quantum walks are the quantum analog of random walks. They are a coherent model of transportation on graphs and a universal model of quantum computation [1, 2], formulated both in continuous and discrete-time. Continuous-time quantum walks (CTQWs) evolve on the space spanned by the vertices of a graph whose structure is encoded in an Hamiltonian [3]. As for discrete-time quantum walks (DTQWs), they require the use of a coin to guide the displacements, which enlarges the Hilbert space of the system [4]. Both formalisms are fundamental quantum computing tools as they serve for quantum simulation of fundamental physics [5–9] and quantum field theory [10–12], quantum information processing and quantum algorithms [13, 14]. Among their algorithmic applications, few examples are related to optimization problems [15–20], quantum state preparation [21–23], machine learning tasks [24–27] or graph related problems [28–30]. Moreover, it has been proved that some DTQWs converge to the Dirac [31–35] and the Schrödinger [36] equations in their continuous limit.

The task of finding a marked element in an unstructured database is known as spatial search. Naturally, the database is modeled as a graph whose vertices and edges respectively represent its elements and their relationships. The most famous related result is Grover's algorithm [37] which requires $\mathcal{O}(\sqrt{N})$ calls to an oracle to find an element among N in an unstructured database.

This algorithm is optimal if the oracle is given as a black box [38] and was surprisingly shown to be a naturally occurring phenomenon [39]. However, when the inner structure of the oracle is known, a classical quantum-inspired algorithm can potentially solve the search problem exponentially faster by simulating the oracle several times [40]. The associated complexity depends on the cost of a single simulation. Moreover, the search problem can be expressed as a quantum walk evolution on graphs, both in discrete [41] and continuous-time [42], each resulting in a quadratic speedup on arbitrary graphs [43, 44].

Quantum walks in open quantum system can be modeled by Quantum Stochastic Walks (QSWs), which are a generalization of CTRWs and CTQWs [45]. They were first introduced as a tool to study the transition between classical and quantum random walks. QSWs have been proposed as an algorithmic tool for several problems including PageRank [46], decision-making [47], quantum state discrimination [48], or function approximation and classification [49]. A discrete-time QSW scheme has also been proposed by Schuhmacher et al. [50]. QSWs have been accurately produced experimentally with a three-dimensional photonic quantum chip [51] and could generally be implemented with the method proposed by Ding et al. for simulation of open quantum systems [52]. Using the QSWs framework, Caruso has numerically shown that for several graphs, transfer efficiency from an arbitrary vertex to an absorbing vertex, named the sink, is optimal when dynamics is 90% coherent and 10% incoherent [53]. Moreover, Caruso et al. have experimentally implemented a photonic maze from which a single photon must escape, and they recovered the same result: the walker finds his way out faster to the sink when 10%

* ugo.nzongani@lis-lab.fr

† andrea.simonetto@ensta.fr

‡ giuseppe.dimolfetta@lis-lab.fr

of the dynamics is non-unitary [54]. These results suggest that a controlled amount of non-unitary dynamics, which may be interpreted as noise, can improve transfer efficiency from an arbitrary set of vertices to a sink. Lastly, maze solving in open quantum systems has also been studied with QSWs assisted by reinforcement learning [55] or with a Grover walk that makes use of sink vertices [56].

In this article, we use continuous-time dynamics to tackle a modified version of the search problem for single marked element. We introduce the Stochastic Quantum Walk Search (SQWS) monitored by a weighted Lindbladian. The unitary evolution is induced by Childs and Goldstone's CTQW search Hamiltonian [42], and non-unitary dissipation is designed to implement a CTRW search dynamics. In addition, we use a trapping sink vertex as an extra dissipative tool, which we only connect to the target vertex of the search with an irreversible transition. Although this is a search problem, we do not quantify performance by the time taken to reach the marked element as a function of graph size as often done, but by the transfer efficiency to reach the trapping site. This metric measures both the amount of information present in the sink and the time needed to reach it. It has already been used as a measure of transport quality in previous works [53, 55, 57, 58], and verified experimentally [54]. In this work, we are interested in a transport problem, not a computational one, and we use the search problem as a case study. The walker starts from a uniform superposition over the vertices of the graph and has to reach the trapping site by moving through a search-driven dynamics guiding it to the target vertex. We numerically show that a mix of unitary and non-unitary operations can outperform a fully coherent or incoherent dynamics for reaching the sink. The balance between unitary and non-unitary operations is controlled with a tunable mixing parameter. The performance of the hybrid regime depends on the graph topology and the connectivity of the target vertex. We show that an increase of non-unitary operations may be compensated by increasing the strength of the quantum walk exploration, at the cost of reducing the importance of the searching oracle that marks the target vertex. Moreover, we show that the addition of non-unitary operations leads to an improvement of performance only in the presence of a sink. Lastly, we relate the best mixing parameter of unitary and non-unitary dynamics to the system's entropy decay rate. We interpret the hybrid regime as a noisy-assisted quantum evolution as it contains non-unitary operations, even if does not model realistic hardware noise.

We start by introducing different continuous-time dynamics on graphs and the search problem of a single element in Sec. II. We present our model for the modified version of the search problem and our results in Sec. III.

II. PRELIMINARIES

A. Continuous-time dynamics

1. Random Walks

Continuous-time Random Walks (CTRWs) describe the evolution of a single walker on a network modeled by a graph $G = (V, E)$ where V and E are respectively a set of vertices and edges. An unweighted graph is fully described by its adjacency matrix:

$$A_{ij} = \begin{cases} 1 & \text{if } (i, j) \in E, \\ 0 & \text{otherwise.} \end{cases} \quad (1)$$

The CTRW is a Markov process whose rate matrix is the Laplacian $L = D - A$ of the graph, with D a matrix whose diagonal entries are the degree of each vertex. The state of the walker is described by a probability distribution \vec{p} which is a map from V to probabilities. The time evolution of the walker is:

$$\frac{d}{dt}\vec{p}(t) = -L\vec{p}(t). \quad (2)$$

As the column of L sum to zero, an initially normalized probability distribution remains valid under the evolution induced by Eq. (2).

2. Quantum Walks

Continuous-time quantum walks are a coherent model of transportation over complex networks [59]. The walker is represented with a quantum state $|\psi\rangle$ that evolves in an Hilbert space \mathcal{H} spanned by the vertices of the graph. Therefore, the set of vertices V form an orthonormal basis of \mathcal{H} . The time evolution of the walker is given by the Schrödinger equation and the Hamiltonian encodes the structure of the graph:

$$i\hbar \frac{d}{dt} |\psi(t)\rangle = H |\psi(t)\rangle. \quad (3)$$

Throughout, we work in units in which $\hbar = 1$. As the evolution is unitary, the Hamiltonian H has to be Hermitian, making the underlying graph undirected, which is not the case for CTRWs as their underlying graph can have both directed and undirected edges.

3. Quantum Stochastic Walks

The transition from the classical to the quantum regime can be studied with the QSW framework that enables to interpolate between coherent and incoherent dynamics [45]. The state of the walker is described by a density matrix $\rho = |\psi\rangle\langle\psi|$ as the evolution is composed of both unitary and non-unitary operations. The QSWs

evolution is driven by a weighted Lindblad master equation with $\omega \in [0, 1]$:

$$\begin{aligned} \frac{d}{dt}\rho(t) &= -i(1-\omega)[H, \rho(t)] + \omega \sum_{ij} \left(\mathcal{L}_{ij}\rho(t)\mathcal{L}_{ij}^\dagger - \frac{1}{2}\{\mathcal{L}_{ij}^\dagger\mathcal{L}_{ij}, \rho(t)\} \right) \\ &= (1-\omega)\mathcal{U}_H[\rho(t)] + \omega\mathcal{D}_\mathcal{L}[\rho(t)], \end{aligned} \quad (4)$$

where $[\alpha, \beta] = \alpha\beta - \beta\alpha$ and $\{\alpha, \beta\} = \alpha\beta + \beta\alpha$ are the commutator and anti-commutator of operators α and β . The unitary and non-unitary dynamics are respectively encapsulated by \mathcal{U}_H and $\mathcal{D}_\mathcal{L}$, and the parameter ω enables to interpolate between them. A wise choice of Lindblad jump operators \mathcal{L}_{ij} can describe a CTRW evolution [45]. Therefore, for well-defined Lindblad jump operators, the CTQW is recovered for $\omega = 0$ and the CTRW for $\omega = 1$. A linear combination of the two is obtained for other values of ω , leading to a mix between coherent and incoherent dynamics for the walker. It was shown that the introduction of an extra sink vertex in Eq. (4), with $H = A$ and $\mathcal{L}_{ij} = A_{ij}/D_{ij}|i\rangle\langle j|$, leads to an optimal transfer from a set of vertices to this sink vertex when $\omega = 0.1$ for several graphs [53].

B. Spatial Search

1. Random Walk Search

Spatial search expressed as a CTRW evolution consists of a walker spreading over the vertices of a graph until it reaches the marked element m . The marked vertex is an absorbing vertex, meaning that the probability of leaving it is zero. Therefore, the Laplacian has to be modified into an absorbing Laplacian $\hat{L} = \frac{D-\hat{A}}{\|D-\hat{A}\|_2}$ where \hat{A} is the adjacency matrix whose m -th column is the m -th canonical basis vector of $\mathbb{R}^{|V|}$ [60]. The initial state is the uniform probability distribution over the vertices of the graph:

$$\vec{p}(0) = \frac{1}{|V|} \sum_{v \in V} \vec{e}_v, \quad (5)$$

where $\{\vec{e}_v | v \in V\}$ is the set of canonical basis vectors of $\mathbb{R}^{|V|}$.

2. Quantum Walk Search

An optimal quantum walk search algorithm on arbitrary graphs has been introduced by Apers et al. [44]. However, their algorithm implies an expansion of system's Hilbert space as their evolution requires the preparation of an auxiliary Gaussian state. As we do not want to increase the size of the Hilbert space, we use the Hamiltonian introduced by Childs and Goldstone that allows an evolution in the space spanned by the vertices of the graph, even if this framework is not optimal for all

graphs [42]. Thus, the search Hamiltonian is defined as:

$$H_{m,\gamma} = \gamma L - |m\rangle\langle m|, \quad (6)$$

where $\gamma \in \mathbb{R}^+$ determines the strength of the quantum walk exploration induced by L^1 . The initial state is the uniform superposition over the vertices of the graph:

$$|\psi(0)\rangle = \frac{1}{\sqrt{|V|}} \sum_{v \in V} |v\rangle. \quad (7)$$

The heart of the CTQWs spatial search algorithm is to find the minimal value of t and the optimal value of γ to maximize the success probability $|\langle m | e^{-itH_{m,\gamma}} |\psi(0)\rangle|^2$ of finding the marked element. This algorithm was first shown to offer a quadratic speedup over its classical counterparts for the complete graph, the hypercube and the d -dimensional periodic lattice for $d > 4$ [42], and to be optimal for a wide family of graphs by Chakraborty et al. [61]. Lastly, it was shown that quantum walk search performances in this framework can be predicted if certain conditions on the spectral properties of the Hamiltonian driving the walk are met [62].

III. RESULTS

A. Stochastic Quantum Walk Search

1. Model

The SQWS is composed of CTQW and CTRW search dynamics with an additional sink. The sink plays a fundamental role in the system, as we later show that the introduction of non-unitary dynamics improves performance only in its presence. We introduce the sink vertex ϕ and connect it to the target vertex m . The irreversible transition from m to ϕ is modeled by the Lindblad jump operator:

$$\mathcal{L}_{\phi,m}[\rho(t)] = |\phi\rangle\langle m| \rho(t) |m\rangle\langle \phi| - \frac{1}{2}\{|m\rangle\langle m|, \rho(t)\}. \quad (8)$$

Therefore, the evolution of the SQWS is:

$$\begin{aligned} \frac{d}{dt}\rho(t) &= (1-\omega)\mathcal{U}_{H_{m,\gamma}}[\rho(t)] + \omega\mathcal{D}_\mathcal{L}[\rho(t)] + \Gamma\mathcal{L}_{\phi,m}[\rho(t)] \\ &= \mathcal{E}[\rho(t)], \end{aligned} \quad (9)$$

with $\Gamma \in \mathbb{R}^+$ the sink rate and $\mathcal{L}_{ij} = -\hat{L}_{ij}|i\rangle\langle j|$. Thus, the coherent and incoherent dynamics respectively produce a quantum and classical random walks search. The

¹ Note that in the numerical simulations we have normalized the Laplacian so that its eigenvalues are between 0 and 1, thus $L = I - L/\lambda_{\max}$ where λ_{\max} is the highest eigenvalue of L .

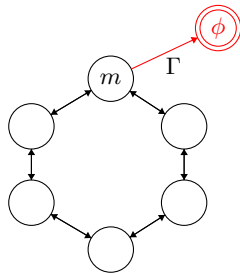


Figure 1: Modified cycle graph C_6 on which we add the extra sink vertex ϕ connected to the target vertex m . The irreversible transition from m to ϕ is weighted with the sink rate Γ . The classical and quantum walk search dynamics only act on the vertices of the initial graph, not on the sink vertex. The search dynamics guides the walker to the target vertex m for it to reach the sink ϕ , and “escape” the graph.

initial state is the uniform superposition over the vertices of the graph (excluding the sink vertex) $\rho(0) = |\psi(0)\rangle\langle\psi(0)|^2$. As an illustration, we show in Fig. 1 a graph with the extra sink vertex ϕ connected to the target vertex m .

In this article, we study the transfer efficiency from an uniform superposition over the vertices to the sink. The walker is guided to the target vertex with a search Hamiltonian, and non-unitary operations designed to implement a CTRW-search, which we interpret as noise. Once on the target vertex, the walker may jump to the sink and remains trapped inside. Starting from a uniform superposition over the vertices, we measure performance with transfer efficiency to the sink (connected only to the marked vertex). The transfer efficiency is defined as [53–55, 57, 58]:

$$E(\omega, \gamma, t) = \frac{1}{t} \int_0^t \text{Tr}(\mathcal{E}[\rho(\tau)] |\phi\rangle\langle\phi|) d\tau. \quad (10)$$

We normalize Eq. (10) so that $E(\omega, \gamma, t) = 1$ corresponds to a total instantaneous transfer of the walker to the sink vertex³, and $E(\omega, \gamma, t) = 0$ that its probability of presence on the sink is zero. As, Eq. (10) considers both success probability and its associated evolution time, it is our unique performance metric. Moreover, we have also executed the SQWS with no sink and show that its presence is mandatory for the hybrid dynamics to beat

² According to our definitions, $\rho(0)$ evolves in a $|V|$ -dimensional Liouville space $\mathcal{B}[\mathcal{H}]$. However, as we add the sink vertex ϕ to the graph, its dimension should be $|V|+1$. By abuse of notation, we assume that all the operators defined in Eq. (9) and $\rho(0)$ act on the $(|V|+1)$ -dimensional Liouville space spanned by the vertices of the graph and the additional sink vertex ϕ .

³ Note that instantaneous transfer of the walker to the sink vertex is not realistic. The value $E(\omega, \gamma, t) = 1$ is just used as an ideal upper bound to evaluate transfer quality.

a fully classical or quantum dynamics. In the absence of sink, the introduction of non-unitary dynamics always reduces performance as we show in Appendix A.

2. Numerical results

We run the SQWS on instances of different graph families and show the results in Fig. 2. We set the time to be linear with the size of the graph as we do not measure performance with computational complexity of reaching the marked element, but with transfer efficiency to the sink. Thus, the value of the maximum evolution time is not as important as for the study of the usual quantum search problem where the optimal performance leads to a quadratic speedup over classical methods. For this reason, we select a large time evolution $t = 10|V|$. Moreover, we set the sink rate to $\Gamma = 1$. For each graph, we run the SQWS for different fixed values of γ , which controls the strength of the quantum walk exploration in Eq. (6). For low values of this parameter, the interaction between the Laplacian and the oracle is balanced, but increasing this value implies reducing or even eliminating the action of the oracle, and thus obtaining a unitary dynamic that only induces a simple quantum walk and not a search dynamic towards the marked vertex. Thus, for high values of γ , the oracle’s action is ignored, eliminating the search dynamic and leading to a free quantum walk. In the following, we use graphs of size $N \in [32, 81]$.

We choose fixed values of $\gamma \in \{0.05, 0.5, 1, 2, 4, 6, 8, 10, 15, 20, 30, 40, 50\}$, taking low and high values to see the impact of the value of this parameter on the transfer efficiency to the sink vertex. We present the main results in Fig. 2 which illustrates the execution of the SQWS on different graphs of 64 vertices, namely, the complete graph K_{64} , the 6-dimensional hypercube Q_6 , the cycle graph C_{64} , the lollipop graph $L_{32,32}$ and the tadpole graph $T_{32,32}$. The lollipop $L_{M,N}$ and tadpole $T_{M,N}$ graphs are respectively the fusion between a complete or cycle graph of size M with a path of size N , we display two instances of these graphs in Fig. 3.

We first observe that for all five graphs, when $\gamma = 0.05$ the quantum regime, i.e. $\omega = 0$, is always the least efficient, with a maximum transfer efficiency of 2%. As we increase the value of the γ parameter, we observe different behaviors depending on the observed graph. We point out that for the complete, the hypercube and the cycle graphs, the search behavior will be the same no matter which vertex is marked, because these graphs are vertex-transitive, i.e. their structure does not allow vertices to be distinguished from each other. For the complete graph, we see that $\gamma = 0.5$ is sufficient to make the quantum regime efficient, with a transfer efficiency of 80%. The quantum regime reaches its maximum efficiency for $\gamma = 2$ with an efficiency of 97%, then increasing γ slightly reduces performance to fall back to 90% when $\gamma = 50$. The hybrid regime exceeds 70% efficiency as early as $\gamma = 0.05$ for $\omega > 0.3$, and increasing

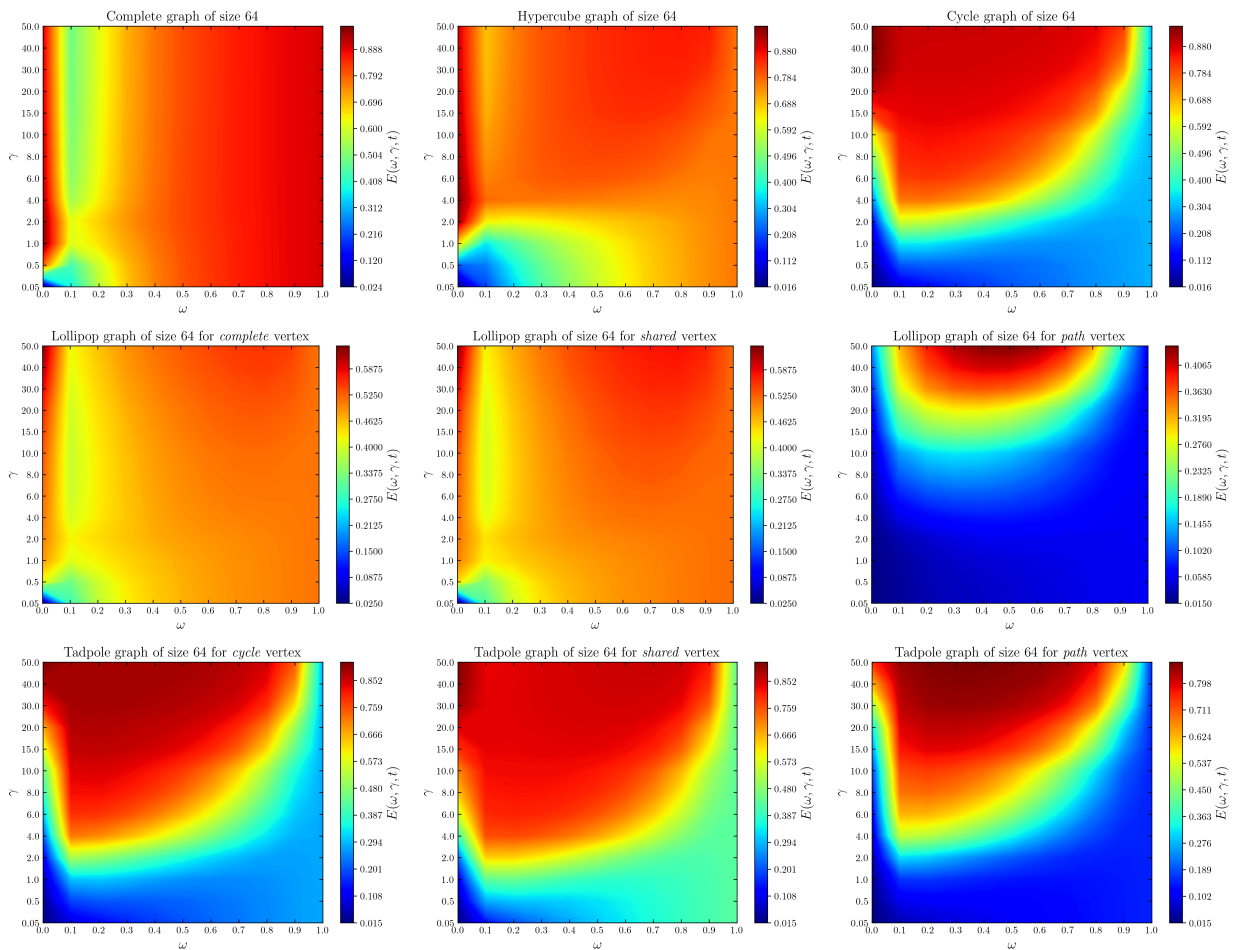


Figure 2: Stochastic Quantum Walk Search (SQWS) performances with different values of $\gamma \in [0.05, 50]$ on graphs of 64 vertices, namely, the complete graph (K_{64}), the 6-dimensional hypercube graph (Q_6), the cycle graph (C_{64}), the lollipop graph ($L_{32,32}$) and the tadpole graph ($T_{32,32}$). The time evolution is set to $t = 640$ units of time. The quantum walk dynamics is recovered for $\omega = 0$, the classical random walk for $\omega = 1$, and a linear combination of the two when $\omega \in]0, 1[$.

γ does not particularly affect performance. In addition, we note an interesting behavior for the hybrid regime: as the value of ω increases, so does the transfer efficiency. This is clearly observed with the lowest performance at $\omega = 0.1$, corresponding to 90% unitary dynamics and 10% non-unitary. Thus, as we increase the importance of non-unitary dynamics, performance improves. However, the purely quantum regime remains the most efficient. For the hypercube, we observe a behavior quite similar to that of the complete graph, in the sense that the purely quantum regime is the most efficient from a low value of γ , namely $\gamma = 4$, and that increasing ω induces a performance improvement for the hybrid regime. However, this phenomenon is less significant than for the complete graph, since this time for $\omega = 0.1$ we obtain a transfer efficiency of over 60% from $\gamma = 2$. However, the hybrid regime for $\omega < 0.6]$ is much less efficient than when $\omega \geq 0.6]$ for $\gamma < 2$, and then performance stabilizes when $\gamma \geq 2$ for the hybrid regime. The case of the cycle

graph is different from the previous ones, as the quantum regime requires a much higher value of γ to outperform the hybrid regime. For example, there is a 50% difference in transfer efficiency at $\gamma = 4$ between the $\omega = 0$ and $\omega = 0.1$ regimes. This difference in performance is reduced with increasing γ , and the $\omega \leq 0.9$ regimes exceed 80% efficiency from $\gamma = 50$. The purely quantum regime becomes the most efficient from $\gamma = 20$ and reaches a maximum transfer efficiency of 95% at $\gamma = 40$. Unlike the complete and hypercube graphs, the classical regime, i.e. $\omega = 1$, is not efficient as it only achieves an efficiency of 30%. Furthermore, we observe that for the cycle graph the increase of ω leads to a reduction in performance unlike in the previous cases. For the lollipop graph, we have run the SQWS on three different vertices that we call *complete*, *shared* and *path*. The *complete* vertex is an arbitrary vertex of the complete graph and *shared* is the vertex shared by the complete and path graphs. We also point out that the performance of the SQWS on

the path graph is similar to that obtained with the cycle and we present these results in detail in Appendix B. The search results obtained for these two vertices are practically similar, and very different from those for the complete graph seen above. In fact, the introduction of a path graph into the complete graph completely alters performance. Transfer efficiency does not exceed 65% for this graph no matter the marked vertex. By way of comparison, the usual complete graph reaches an efficiency of 97% for $\gamma = 2$. The *path* vertex is located at the extreme end of the path graph, and its search gives different results. Whatever the value of γ , transfer efficiency to the sink does not exceed 45%. Searching the *path* vertex is even less efficient than searching the *complete* and *shared* vertices, since the 20% efficiency threshold is exceeded at $\gamma = 15$ and the 40% threshold at $\gamma = 40$. Moreover, the quantum regime does not exceed 12% and the classical one is at 5% efficiency. Lastly, the hybrid regime is more efficient than the quantum one, with a difference of 31% in efficiency when $\gamma = 50$ between the quantum case and the hybrid for $\omega \in [0.3, 0.6]$. Finally, we ran the SQWS on the tadpole graph on the vertices *cycle*, *shared* and *path*. The vertex *cycle* is located on the cycle in such a way as to maximize the distance to *shared*. Unlike the previous case of the lollipop, which was made up of two graphs with very different reactions to the increase in the γ parameter, the tadpole graph is a fusion of two graphs with the same reaction to it (the cycle and path graphs). The SQWS behaves approximatively the same way for all three vertices, the hybrid regime performs much better than the quantum regime for certain γ values. In particular, we note that, depending on the vertex sought, the value of γ required for the quantum regime to be at least as efficient as the hybrid varies. The vertex *shared* is the one requiring the lowest value of γ for this, followed by *cycle* and finally *path*. In addition, we observe that for the *path* vertex, the hybrid regime has more difficulty compensating for the increase in ω by increasing γ . Still for this vertex, the quantum regime is not the most efficient even for $\gamma = 50$, unlike the other two vertices. Finally, we see that for this graph, the classical regime performs best when searching for the *shared* vertex.

In this study, we recover the results of Caruso et al. [53, 54] as the value $\omega = 0.1$ is critical for graphs where the hybrid regime outperforms the quantum one. In these cases, we observe that the mixing $\omega = 0.1$ is the first hybrid regime to outperform quantum dynamics. Moreover, we generalize their result by adding a new parameter γ and showing that the topology of the graph plays a major role in the performance of the SQWS. The parameter γ plays a fundamental role as it allows to control the strength of quantum walk exploration. However, we see that an increase of γ reveals a new spectrum of the hybrid behavior as the increase of ω can be compensated with an increase of γ . However, an increase in γ tends to reduce the importance of the oracle that marks the searched vertex and thus produce dynamics more centered on a quantum walk free rather than a search quan-

tum walk. Generally speaking, the SQWS behaves in a number of interesting ways, depending on the graph topology and the target vertex connectivity. The first behavior is the possibility for a hybrid regime to outperform quantum and classical dynamics for this modified search problem. We also note that in some cases, a low-noise hybrid regime (low value of ω) is less efficient than a noisier hybrid regime. This phenomenon is clearly observed for the complete graph, but also in a lighter way for the hypercube and lollipop (for the *complete* and *shared* vertices) graphs. Finally, we see that increasing the value of γ can compensate for the increase in the interpolation parameter ω . In other words, increasing the importance of graph exploration for the walker, and thus neglecting the oracle that enables the search, offsets the increase in the importance of incoherent operations in the system.

Intuitively, we can use metrics in an attempt to understand why the SQWS behaves differently on different graphs, and even on different vertices belonging to the same graph. A useful global graph metric is its density, with the densest complete graph serving as a reference with a density of 1. Then, two interesting local metrics for the target vertex are its eccentricity, i.e. the longest of the shortest paths to reach that vertex from any vertex in the graph, and its degree centrality, which indicates how connected the vertex is in the graph. A centrality of 1 means that the vertex is connected to all the others, and 0 to none. Interestingly, density and eccentricity are equal quantities for vertex transitive graphs, i.e. graphs whose structure does not allow vertices to be distinguished from each other. We show all these characteristics for all the graphs on which we have run the SQWS on Table I. We can see that all the graphs where the hybrid out regime performs the quantum regime for certain values of γ have a high eccentricity, i.e. which scales in $\mathcal{O}(N)$. Among these graphs (cycle, path, maze, lollipop, tadpole) we also observe that the higher the eccentricity and the lower the centrality of the target vertex, then the purely quantum regime requires a higher value of γ to outperform the hybrid. Furthermore, we see that the lower the eccentricity and centrality, the lower the value of γ required for the quantum regime to perform. Finally, it seems that the higher the density and centrality, the less an increase in γ can compensate for the introduction of incoherent dynamics into the search.

We explore the behavior of the SQWS on many different families of graphs, and observe how it behaves when a cycle is gradually transformed into a complete graph in Appendix B.

B. Relation to entropy

We now relate the optimal interpolation regime ω to the evolution of the Von Neumann entropy of the system:

$$S(\rho) = -\text{Tr}(\rho \ln \rho). \quad (11)$$

Table I: Global (density) and local metrics (degree centrality and eccentricity) of the target vertex for the different graphs on which we have run the Stochastic Quantum Walk Search (SQWS).

Graph	Size	Density	Target vertex	m	Degree centrality	Eccentricity
Complete K_N	$N = 64$	1	-	-	1	$1 = \mathcal{O}(1)$
Cycle C_N	$N = 64$	0.0317	-	-	0.0317	$32 = \lfloor N/2 \rfloor = \mathcal{O}(N)$
d -Hypercube Q_d	$N = 2^d = 64$ ($d = 6$)	0.0952	-	-	0.0952	$6 = d = \mathcal{O}(\log N)$
Grid $G_{\sqrt{N} \times \sqrt{N}}$	$N = 81$	0.0444	<i>center</i>	-	0.05	$8 = \sqrt{N} - 1 = \mathcal{O}(\sqrt{N})$
			<i>border</i>	-	0.025	$16 = 2(\sqrt{N} - 1) = \mathcal{O}(\sqrt{N})$
Star S_{N-1}	$N = 64$	0.0312	<i>center</i>	-	1	$1 = \mathcal{O}(1)$
			<i>border</i>	-	0.0158	$2 = \mathcal{O}(1)$
Wheel W_N	$N = 64$	0.0625	<i>center</i>	-	1	$1 = \mathcal{O}(1)$
			<i>border</i>	-	0.0476	$2 = \mathcal{O}(1)$
Perfect Binary Tree	$N = 2^{d+1} - 1 = 63$	0.0317	$d_m = 0$ (<i>root</i>)	-	0.0322	$5 = d + d_m = \mathcal{O}(\log N)$
			$d_m = 3$	-	0.0483	$8 = d + d_m = \mathcal{O}(\log N)$
PBT_d of depth d	$(d = 5)$	0.0317	$d_m = 5$ (<i>leaf</i>)	-	0.0161	$10 = d + d_m = \mathcal{O}(\log N)$
			<i>center</i>	-	0.0312	$32 = \lfloor N/2 \rfloor = \mathcal{O}(N)$
Path P_N	$N = 65$	0.0307	<i>border</i>	-	0.0156	$64 = N - 1 = \mathcal{O}(N)$
			<i>complete</i>	-	0.4920	$33 = N + 1 = \mathcal{O}(N)$
Lollipop $L_{M,N}$	$M+N=32+32$	0.2619	<i>shared</i>	-	0.5079	$32 = N = \mathcal{O}(N)$
			<i>path</i>	-	0.0158	$33 = N + 1 = \mathcal{O}(N)$
			<i>cycle</i>	-	0.0317	$48 = N + \lfloor M/2 \rfloor = \mathcal{O}(N+M)$
Tadpole $T_{M,N}$	$M+N=32+32$	0.0317	<i>shared</i>	-	0.0476	$32 = \max(N, \lfloor M/2 \rfloor) = \mathcal{O}(N+M)$
			<i>path</i>	-	0.0158	$48 = N + \lfloor M/2 \rfloor = \mathcal{O}(N+M)$
			<i>HC</i>	-	0.1846	6
Random (Small-World)	$N = 66$	0.0867	<i>IC</i>	-	0.0923	6
			<i>LC</i>	-	0.0615	5
			<i>exit</i>	-	0.0273	34
Maze M_N	$N = 73$	0.0138	-	-	0.0273	34

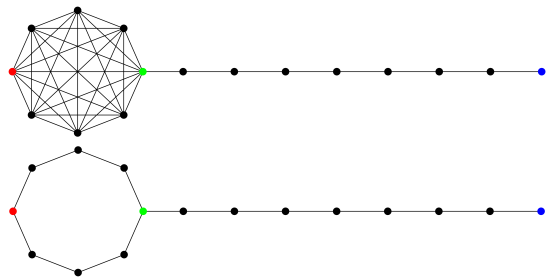


Figure 3: Instances $L_{8,8}$ and $T_{8,8}$ of the lollipop (upper) and tadpole (lower) graphs, that are respectively a fusion between the complete graph K_8 or the cycle graph C_8 with the path graph P_8 . We respectively refer to the locations of the red, green and blue vertices as *complete*, *shared* and *path* vertices for the lollipop graph, and *cycle*, *shared* and *path* for the tadpole graph.

We observe for every run of the SQWS that the entropy first increases up to a maximum, and then decreases until it converges to zero. We also observe that when an increase in the maximum value of γ increases the performance of the SQWS, i.e. the transfer to the sink, this translates into a reduction in the time needed to reach the entropy maximum and a faster convergence to zero thereafter. Furthermore, we observe that the optimal interpolation regime ω is that whose entropy converges to zero the fastest. The presence of the sink vertex ϕ introduces dissipation in the system, therefore, as $t \rightarrow \infty$ the walker will end up in the sink with a probability of 1. Thus, the state of the walker converges from $\rho(0)$ to the projector $|\phi\rangle\langle\phi|$. Although zero entropy indicates a pure state, it does not guarantee that this state is the state

towards which the system converges. Therefore, we also compute the l_1 -norm coherence, which is the sum of the off-diagonal elements of ρ :

$$C_{l_1}(\rho) = \sum_{i \neq j} |\rho_{ij}|. \quad (12)$$

As the initial state is the uniform superposition over the set of vertices V , the initial value is $C_{l_1}(\rho(0)) = |V| - 1$. For all graphs on which we run the SQWS, we observe that this quantity decreases monotonically and it converges to zero. Thus, the convergence of entropy to zero does indicate that the walker state is getting closer and closer to the state $|\phi\rangle\langle\phi|$, as ρ becomes increasingly diagonal over time. We illustrate the entropy evolution over time in Fig. 4 for the complete, the hypercube, the cycle and the lollipop (for the *path* vertex) graphs.

Looking at Fig. 4, we can see that the choice of γ has an impact on the evolution of entropy. For the complete graph on Fig. 4a, we can see that for $\gamma = 0.05$ the entropy that decreases most rapidly is obtained for $\omega = 1$, which can be verified with Fig. 2. Furthermore, we observe that for $\omega = 0$ entropy increases only very slightly and does not decrease. This is simply because the chosen evolution time is not long enough to observe this phenomenon. We also observe that the $\omega = 0.1$ regime is the worst for all choices of γ except for $\gamma = 0.05$ where the quantum case is the worst. We can see that entropy decreases most rapidly in the quantum case, i.e. $\omega = 0$, when $\gamma = 2$. This can also be seen in Fig. 2, as we can see that for the γ values selected, the best transfer efficiency for the complete graph is obtained for $\gamma = 2$. For the hypercube on Fig. 4b, we also observe that for $\gamma \leq 1$, the best-performing regimes are $\omega \in [0.5, 1]$ as their entropy decreases most rapidly. From $\gamma = 2$ onwards, we observe that the entropy of the quantum regime decreases most rapidly, and this rate of decay increases as we move on to $\gamma = 4$. For $\gamma = 50$ we see that the quantum regime still has the fastest decaying entropy, but this decay is slower than for $\gamma = 4$, for example, as performance is less good, as can be seen in Fig. 2. Moreover, when $\gamma = 50$ we observe that the purely classical regime, i.e. $\omega = 1$, has the slowest decaying entropy after $\omega = 0.1$ and $\omega = 0.2$. For the cycle graph case, we can see from Fig. 4c that when $\gamma = 15$ the quantum regime is still less efficient than most hybrid regimes and the classical case. This graph requires higher values of γ to accelerate the rate of entropy decay than the complete and hypercube graphs. Finally, for the lollipop where we mark the *path* vertex, we observe that an increase in γ has little impact on the rate of entropy decay. In particular, we see that the quantum regime does not reach its entropy maximum and thus does not start to decay entropy even for high values of the γ parameter. The hybrid regime, on the other hand, is affected, albeit only slightly. Looking at Fig. 2, we see that for this graph, when searching for the *path* vertex, the increase in γ only starts to have an effect at $\gamma = 15$, reaching a maximum of just 40% transfer efficiency.

In general, we can clearly see from Fig. 4 that the efficiency of transfer to the sink translates firstly into a reduction in the time t_S needed to reach maximum entropy. Then, by a convergence of entropy towards zero as quickly as possible, where the ω -regime maximizing efficiency is the one with the fastest convergence.

We also illustrate the reduction of duration t_S required to reach the maximum entropy in Fig. 5 for these graphs. For the complete graph, we can clearly see that this duration t_S is minimal for low values of γ and then increases again as we increase the value of γ , as an increase in this parameter reduces transfer efficiency. This phenomenon is particularly marked for $\omega \in [0, 0.1]$. We point out that the evolution of t_S is constant for the classical case for all graphs, i.e. $\omega = 1$, as the parameter γ lies in the Hamiltonian. We observe much the same behavior in the evolution of time t_S for the hypercube, with a sharp decrease followed by an increase as γ increases. For both graphs, the best value of γ is low, so higher values increase the time needed to reach the entropy maximum before the entropy decreases. For the cycle and the lollipop graphs, we observe a monotonic decay of t_S as γ increases because for these graphs, an increase in γ translates into an improvement in transfer efficiency. In addition, for the lollipop graph, the duration t_S for the quantum regime is constant because, as mentioned above, entropy does not reach its maximum with the evolution time we have used. Therefore, given a value of γ , we observe that the optimal interpolation regime ω in our framework is the one that leads to the fastest convergence to zero entropy. Furthermore, an increase in the value of γ can improve the SQWS performance if it results in a significant reduction in the time needed to reach maximum entropy.

IV. CONCLUSION

In summary, we have studied a continuous-time search problem in which the walker explores a graph according to a searching dynamics driven to a specific target vertex. We also connected a trapping sink vertex to the target with an irreversible transition. We were interested in the transfer efficiency of a slightly modified search problem, and not in its computational complexity of the search problem. We extended the result of Caruso et al. [53, 54] to a Stochastic Quantum Walk Search (SQWS) and we numerically showed that a tunable mixing of unitary and non-unitary dynamics can lead to a better transfer efficiency than a non-hybrid evolution for this problem depending on (i) the graph topology, (ii) the target vertex connectivity and (iii) a parametrized Hamiltonian. In particular, the Hamiltonian parameter controls the strength of the quantum walk exploration, its increase reduces or even eliminates the impact of the oracle and therefore the search feature. We have also related the optimal tunable mixing of unitary and non-unitary operations to the system entropy decay rate. Moreover, we have shown that the hybrid regime can beat the purely

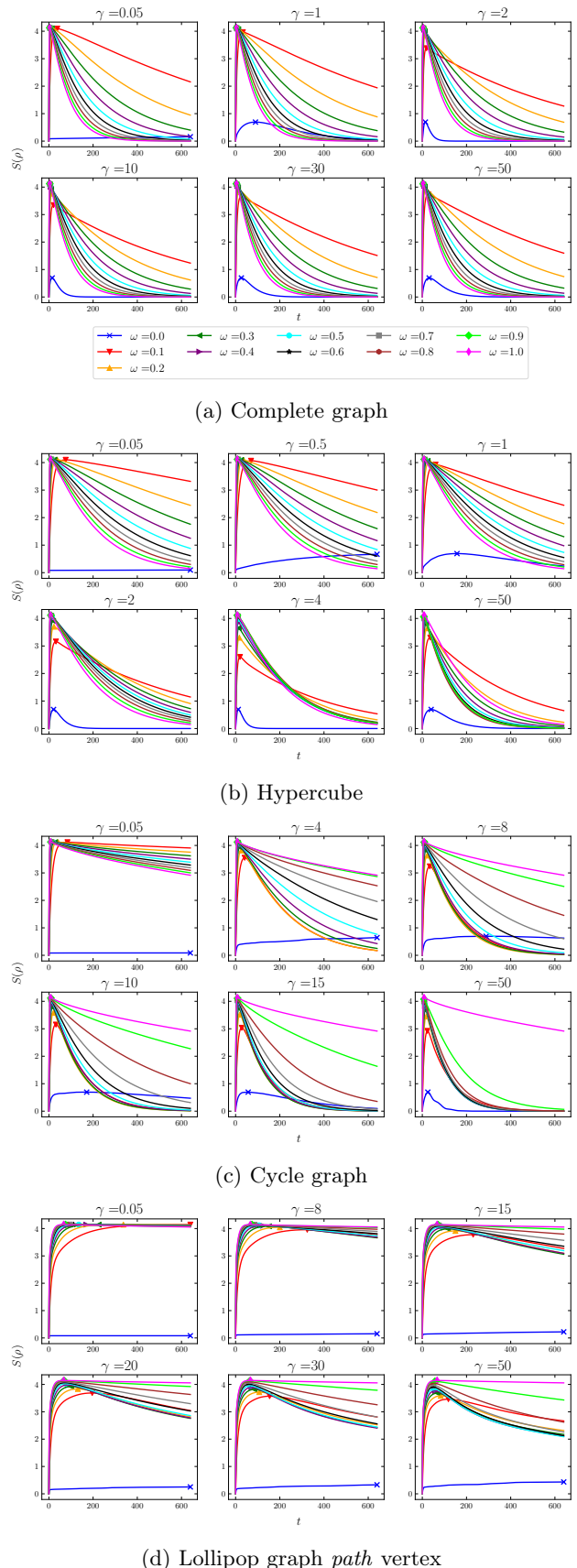


Figure 4: Von Neumann entropy $S(\rho)$ as a function of time t for different values of γ for the complete graph K_{64} , the 6-hypercube Q_6 , the cycle graph C_{64} and the lollipop graph $L_{32,32}$ for the *path* vertex. The markers indicate the time t_S at which the entropy reaches its maximum value before decreasing down to zero.

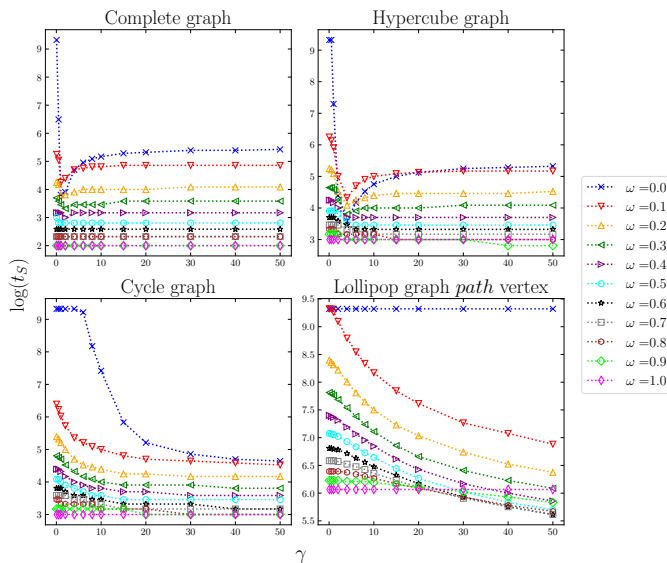


Figure 5: Evolution of the duration t_S needed to reach maximum entropy as a function of γ for the complete graph K_{64} , the 6-hypercube Q_6 , the cycle graph C_{64} and the lollipop graph $L_{32,32}$ (with *path* vertex) for different values of interpolation $\omega \in [0, 1]$.

quantum dynamics only in the presence of a trapping sink. For numerous graphs, mostly sparse, quantum evolution requires to increase the Hamiltonian parameter to achieve the same performance. Therefore, by considering the value of this parameter as a computational resource, the hybrid evolution may require fewer resources than the quantum to perform. More importantly, at a fixed parameters configuration, we can still play with the interaction graph to fit the optimal transfer performance. This can pave the way to a technological leap where noise can be seen as a useful physical resource, in a hardware setting where one can change the connectivity of the architecture for reliable quantum computing. In conclusion, future work could also focus to provide a natively circuit based model for the above results, introducing quantum noise as close as possible to real physical devices’.

V. DATA AVAILABILITY

Simulations were carried out with the Python library QuTip [65] and the graphs were generated with NetworkX [66]. The code is available at: [SQWS](#).

VI. ACKNOWLEDGEMENTS

We thank Ravi Kunjwal, Joachim Tomasi, Julien Zylberman and Sunheang Ty for their usefull feedback on the form and content of this manuscript. This work is supported by the PEPR EPiQ ANR-22-PETQ-0007, by the ANR JCJC DisQC ANR-22-CE47-0002-01.

Appendix A: SQWS with no sink

In this section, we briefly discuss the performances of the SQWS with no use of an extra sink vertex connected to the target vertex. We set $\Gamma = 0$ in Eq. (9). This setting corresponds to the usual quantum search problem when $\omega = 0$ as the success probability is now related to the presence of the walker in the target vertex m instead of the sink. We use Simulated Annealing [64] to find the best value γ^* that maximizes the usual spatial search success probability:

$$P(\omega, \gamma, t) = \text{Tr}(\mathcal{E}[\rho(t)] |m\rangle \langle m|). \quad (\text{A1})$$

Childs and Goldstone search provides a quadratic speedup for the complete graph and the hypercube [42], meaning that the evolved state $\mathcal{E}[\rho(t)]$ reaches a large overlap with the target $|m\rangle \langle m|$ in a timeframe that scales as $t = \mathcal{O}(\sqrt{|V|})$, which is not the case for the cycle graph [62]. Therefore, we run the SQWS on instances of the complete graph, the hypercube and the cycle graph and show the results in Fig. 6. Unsurprisingly, the introduction of non-unitary operations, i.e. increasing the value of ω , drastically reduces search performance. For the complete graph and the hypercube, we still observe a peak reached in a time scaling quadratically with their size when $\omega \leq 0.4$. However, the maximum amplitude reached is much lower than that obtained for the purely unitary evolution, i.e. $\omega = 0$. Furthermore, for the complete graph and the hypercube, once $\omega > 0.4$, we observe a change in behavior. As there is no longer any oscillatory behavior and we get that $\gamma^* = 0$, the success probability suddenly converges to 1. However, the time taken to approach 1 no longer scales quadratically with the size of the graph. As for the cycle graph, it is clear that the search does not work even for the quantum case. There is a slight oscillation as long as $\omega \leq 0.3$, then a jump in performance from $\omega = 0.4$. However, when $\omega \in [0.4, 1]$, although the maximum amplitude reached continues to increase, it follows a very slow growth rate, not exceeding 0.3 when those of the complete graph and the hypercube are very close to 1.

Therefore, we can see that simply removing the sink term completely changes the reaction of the SQWS to the introduction of non-unitary operations. In the presence of a sink, the transfer to the sink can be much more efficient in a noisy regime than in a purely quantum one, based on the graph topology, the target vertex connectivity, and the value of γ . Hence, the addition of non-unitary operations is not usefull if the graph does not have an extra trapping site.

Appendix B: SQWS with sink

In this section, we take the numerical study of the SQWS a step further by running it on numerous instances of different graph families.

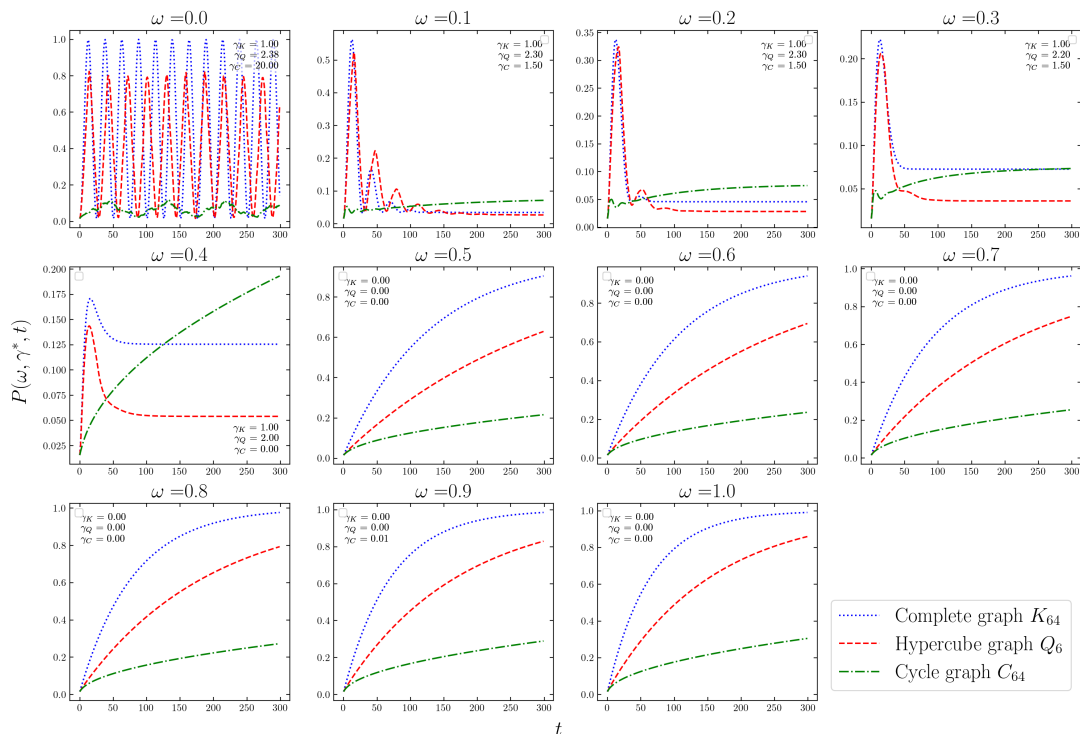


Figure 6: Probability $P(\omega, \gamma^*, t)$ over time of finding the target vertex using the Stochastic Quantum Walk Search (SQWS) with no sink vertex connected to the target vertex, i.e. $\Gamma = 0$ in Eq. (9), on the complete graph (K_{64}), the 6-dimensional hypercube (Q_6) and the cycle graph (C_{64}). The usual quantum walk search is recovered for $\omega = 0$, the classical random walk search for $\omega = 1$, and a linear combination of the two when $\omega \in]0, 1[$.

1. Additional graphs

We now run the SQWS exclusively on non-vertex transitive graphs, i.e. graphs with a structure that distinguishes their vertices, of sizes $N \in [63, 81]$. We select the path graph (P_N), the star graph (S_{N-1}), the wheel graph (W_N), the 2D-grid ($G_{\sqrt{N} \times \sqrt{N}}$), the perfect binary tree of depth d (PBT_d), a maze graph⁴ (M_N) and a random graph (SW_N) constructed by gluing together three small-world graphs of 22 vertices each with different average connectivity and rewiring probabilities [67]. We show the graph SW_{66} in Fig. 8 and the results of the SQWS on these graphs in Fig. 7. For the maze we mark the *exit* vertex and for the path, the *center* and one of the two end vertices, which we call *border*. The behavior of the maze and path graphs is similar to that of the cycle observed in Fig. 2. The hybrid regime outperforms the quantum one up to a certain value of γ . Moreover, we note that this critical value, where quantum outperforms hybrid, is highest when searching for a vertex located at

the path extremity. We also note that this vertex has the highest eccentricity of all the vertices on which we have run the SQWS (see Table I). For these two graphs, an increase in γ compensates for the increase in ω , as the hybrid regime performs almost as well as the quantum one for high values of γ . For the star and wheel graphs, unsurprisingly, we obtain very different behavior depending on the marked vertex. When searching for the central vertex, the transfer efficiency is very high from $\gamma = 0.05$ except for $\omega \in [0, 0.2]$. Indeed, for $\omega > 0.2$ we already obtain an efficiency of over 70% for both graphs. The $\omega \in [0, 0.2]$ regimes exceed 70% efficiency from $\gamma = 1$ and the quantum regime also becomes the best for $\gamma = 1$. It can be seen that both graphs react similarly to an increase in γ to compensate for the increase in ω . For both graphs, the increase in γ ends up slightly reducing performance for $\omega \in [0, 0.8]$, and the wheel graph is slightly more affected by this reduction in performance. However, if we do not search for the central vertex, the behavior of the SQWS changes completely. This time, a much higher value of γ is required to achieve an efficiency of around 90%. Above a certain value of γ , approximately 30 for the star and 15 for the wheel, the quantum regime outperforms the hybrid. We also observe that it is more difficult to stabilize hybrid performance with the increase of ω for the star than for the wheel graph. Finally, the behavior of the SQWS on the remaining graphs, i.e. the

⁴ Maze generation can be easily done using Depth-First Search (DFS) on a grid. Once the maze is created, each cell is considered as a vertex, and two vertices are adjacent if there is no wall between their respective cells.

2D-grid, the perfect binary tree and the random graph composed of three small-world graphs, are quite similar. In each case, the quantum regime becomes more efficient than the hybrid for low values of $\gamma < 10$. We note, however, that the grid is the graph for which the hybrid best compensates for the increase in non-unitary dynamics by the increase in γ , especially when the marked vertex is at one of the extremities. This compensation is least present for the binary tree when searching for the vertex located at depth 5, i.e. the leaf. In this case, the hybrid regime struggles to catch up with the performance of the quantum one once it has passed it. Furthermore, it is for the search of this vertex that the quantum regime requires the highest value of $\gamma = 15$ to exceed 80% efficiency among these last three graphs. Moreover, for the root search, we observe one of the same phenomenon as for the complete graph, i.e. that a low-noise regime is less efficient than a noisier one. Finally, the search on the random graph gives rather equivalent results for the three vertices searched. The quantum regime exceeds 80% efficiency for very low values of $\gamma < 6$, then increasing this same parameter compensates for the increase in ω . As in the case of the binary tree, we can see that the higher the connectivity of the vertex we are looking for, the more efficient the high-noise regime is compared to the low-noise one, although the difference is very small compared to what we observed for the complete graph.

2. Ring-lattice transition

As the results on the cycle and the complete graphs are completely different, we use the Ring-lattice graph model to progressively transform a cycle into a complete graph. A ring-lattice graph also known as a k -cycle is the basis of Watts and Strogatz model widely known as small-world networks [67]. It consists of a cycle graph where each vertex is connected to its k nearest neighbors. Therefore when $k = 2$ we recover a cycle graph and the maximum value of k generates a complete graph. As an illustration we show the transition from the cycle to the complete graph of size $N = 8$ in Fig. 9. We run the SQWS on the Ring-lattice graph of size $N = 32$ for 16 different values of k , the cycle graph is obtained for $k = 2$ and the complete graph for $k = 32$. We present the results in Fig. 11. As k increases, the eccentricity of the marked vertex decreases as the graph's connections increase, leading to an increase in its centrality as shown in Fig. 10. We observe that the hybrid regime outperforms the purely quantum one only for the cycle graph, i.e. $k = 2$. A slight increase in connectivity allows the quantum regime to gain the upper hand over the hybrid, as we can see that from $k = 4$ the hybrid regime is no more efficient than the purely quantum one for low values of γ . We then note that as the value of k increases, the low-noise hybrid regime, i.e. low value of ω , is less efficient than a noisier hybrid. This feature was clearly visible for the complete graph K_{64} in Fig. 2.

-
- [1] N. B. Lovett, S. Cooper, M. Everitt, M. Trevers, and V. Kendon, *Physical Review A* **81**, 042330 (2010).
 - [2] A. M. Childs, *Physical Review Letters* **102** (2009), ISSN 1079-7114, URL <http://dx.doi.org/10.1103/PhysRevLett.102.180501>.
 - [3] E. Farhi and S. Gutmann, *Phys. Rev. A* **58**, 915 (1998), URL <https://link.aps.org/doi/10.1103/PhysRevA.58.915>.
 - [4] Y. Aharonov, L. Davidovich, and N. Zagury, *Physical Review A* **48**, 1687 (1993).
 - [5] K. Bepari, S. Malik, M. Spannowsky, and S. Williams, *Physical Review D* **106**, 056002 (2022).
 - [6] P. Arnault and F. Debbasch, *Physical Review A* **93**, 052301 (2016).
 - [7] F. De Nicola, L. Sansoni, A. Crespi, R. Ramponi, R. Osellame, V. Giovannetti, R. Fazio, P. Mataloni, and F. Sciarrino, *Physical Review A* **89**, 032322 (2014).
 - [8] G. Di Molfetta, M. Brachet, and F. Debbasch, *Physica A: Statistical Mechanics and its Applications* **397**, 157 (2014).
 - [9] J. Zylberman, G. Di Molfetta, M. Brachet, N. F. Loureiro, and F. Debbasch, *Physical Review A* **106**, 032408 (2022).
 - [10] *New Journal of Physics* **18**, 103038 (2016).
 - [11] N. Eon, G. Di Molfetta, G. Magnifico, and P. Arrighi, *Quantum* **7**, 1179 (2023).
 - [12] K. Sellapillay, P. Arrighi, and G. Di Molfetta, *Scientific Reports* **12**, 2198 (2022).
 - [13] K. Kadian, S. Garhwal, and A. Kumar, *Computer Science Review* **41**, 100419 (2021).
 - [14] M. Roget and G. Di Molfetta, in *Asian Symposium on Cellular Automata Technology* (Springer, 2024), pp. 72–83.
 - [15] S. Schulz, D. Willsch, and K. Michielsen, *Physical Review Research* **6**, 013312 (2024).
 - [16] S. Marsh and J. B. Wang, *Phys. Rev. Res.* **2**, 023302 (2020), URL <https://link.aps.org/doi/10.1103/PhysRevResearch.2.023302>.
 - [17] T. Bennett, E. Matwiejew, S. Marsh, and J. B. Wang, *Quantum walk-based vehicle routing optimisation* (2021), 2109.14907.
 - [18] N. Slate, E. Matwiejew, S. Marsh, and J. B. Wang, *Quantum* **5**, 513 (2021), ISSN 2521-327X, URL <http://dx.doi.org/10.22331/q-2021-07-28-513>.
 - [19] E. Campos, S. E. Venegas-Andraca, and M. Lanzagorta, *Scientific Reports* **11**, 16845 (2021).
 - [20] D. Qu, E. Matwiejew, K. Wang, J. Wang, and P. Xue, *Quantum Science and Technology* **9**, 025014 (2024).
 - [21] Y.-J. Chang, W.-T. Wang, H.-Y. Chen, S.-W. Liao, and C.-R. Chang, *Preparing random state for quantum financing with quantum walks* (2023), 2302.12500, URL <https://arxiv.org/abs/2302.12500>.
 - [22] B. S. Choudhury, M. K. Mandal, and S. Samanta, *International Journal of Theoretical Physics* **63**, 71 (2024).
 - [23] A. Gonzales, R. Herrman, C. Campbell, I. Gaidai, J. Liu, T. Tomesh, and Z. H. Saleem, arXiv preprint

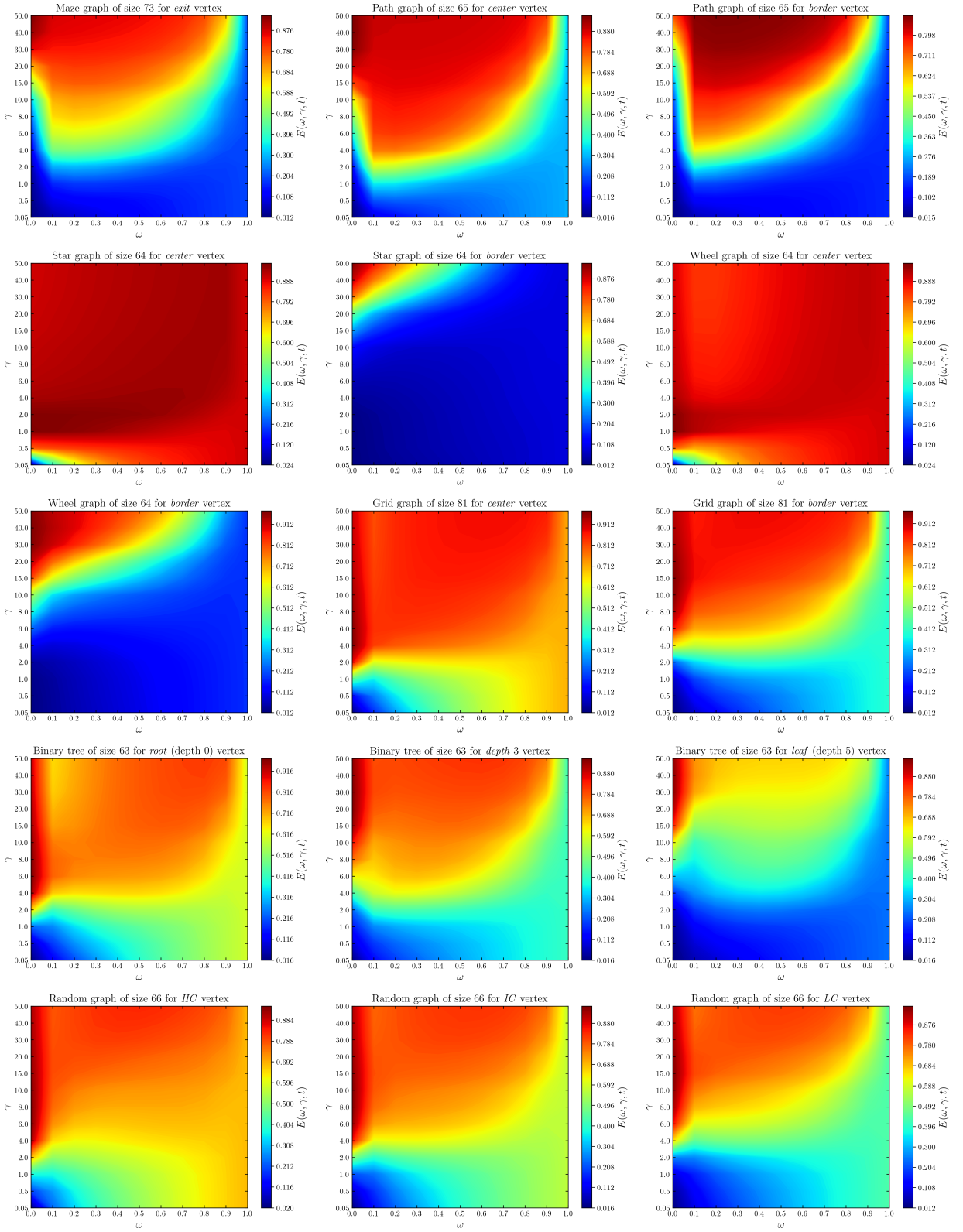


Figure 7: Stochastic Quantum Walk Search (SQWS) performances with different values of $\gamma \in [0.05, 50]$ on a maze graph (M_{73}), the path graph (P_{65}), the star graph (S_{63}), the wheel graph (W_{64}), the 2D-grid ($G_{9 \times 9}$), the perfect binary tree of depth 5 (PBT_5) and a random graph (SW_{66}) which was constructed by gluing together three small-world graphs of size $N = 22$ each with different average connectivity and rewiring probabilities. The time evolution is set to $t = 10N$ units of time, with N the size of each graph. The quantum walk dynamics is recovered for $\omega = 0$, the classical random walk for $\omega = 1$, and a linear combination of the two when $\omega \in]0, 1[$.

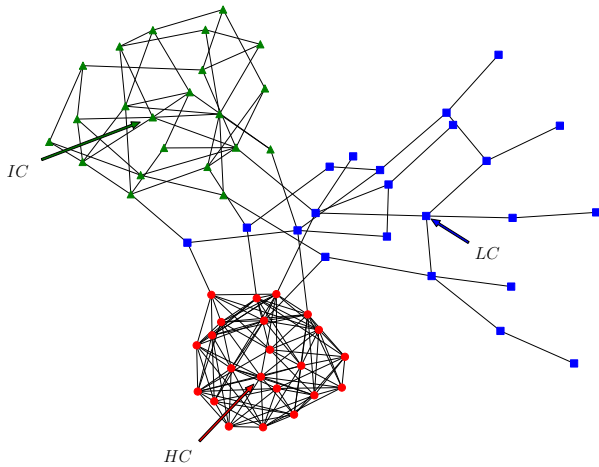


Figure 8: Random graph SW_{66} constructed by gluing together three small-world graphs of size $N = 22$ each with different average connectivity and rewiring probabilities. The target vertices are named HC , IC and LC , respectively for high, intermediate and low connectivity. Their average connectivity are respectively 10, 4 and 3. Their respective rewiring probabilities are 0.1, 0.5 and 0.8.

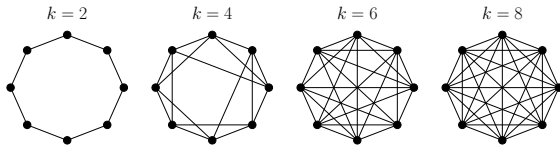


Figure 9: Transition from the cycle graph to the complete graph of size $N = 8$ with the Ring-lattice model. As far as possible, each vertex is connected to its k -nearest neighbors.

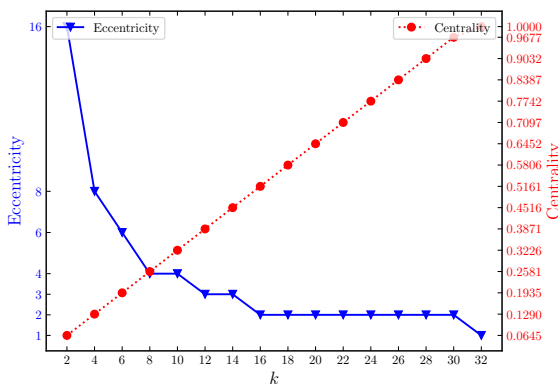


Figure 10: Eccentricity and centrality of the target vertex as a function of k for Ring-lattice graphs of size $N = 32$.

arXiv:2405.20273 (2024).

- [24] W.-M. Shi, Q.-T. Zhuang, Y.-H. Zhou, and Y.-G. Yang, *Multimedia Tools and Applications* **83**, 34979 (2024).
- [25] S. Dernbach, A. Mohseni-Kabir, S. Pal, and D. Towsley, in *Complex Networks and Their Applications VII: Volume 2 Proceedings The 7th International Conference on Complex Networks and Their Applications COMPLEX NETWORKS 2018 7* (Springer, 2019), pp. 182–193.
- [26] L. S. de Souza, J. H. de Carvalho, and T. A. Ferreira, in *2019 8th Brazilian Conference on Intelligent Systems (BRACIS)* (IEEE, 2019), URL <http://dx.doi.org/10.1109/BRACIS.2019.00149>.
- [27] M. Roget, G. Di Molfetta, and H. Kadri, in *Uncertainty in artificial intelligence* (PMLR, 2022), pp. 1697–1706.
- [28] A. M. Childs, R. Cleve, E. Deotto, E. Farhi, S. Gutmann, and D. A. Spielman, in *Proceedings of the thirty-fifth annual ACM symposium on Theory of computing* (2003), pp. 59–68.
- [29] P. Chawla, R. Mangal, and C. M. Chandrashekar, *Quantum Information Processing* **19**, 1 (2020).
- [30] C. Benedetti and I. Gianani, *AVS Quantum Science* **6** (2023).
- [31] P. Arrighi, V. Nesme, and M. Forets, *Journal of Physics A: Mathematical and Theoretical* **47**, 465302 (2014), URL <https://dx.doi.org/10.1088/1751-8113/47/46/465302>.
- [32] G. Di Molfetta and F. Debbasch, *Journal of Mathematical Physics* **53** (2012).
- [33] F. W. Strauch, *Physical Review A—Atomic, Molecular, and Optical Physics* **73**, 054302 (2006).
- [34] U. Nzongani, N. Eon, I. Márquez-Martín, A. Pérez, G. Di Molfetta, and P. Arrighi, *Physical Review A* **110**, 042418 (2024).
- [35] G. Di Molfetta, *Quantum Walks, Limits, and Transport Equations* (IOP Publishing, 2024).
- [36] N. Jolly and G. Di Molfetta, *The European Physical Journal D* **77**, 80 (2023).
- [37] L. K. Grover, in *Proceedings of the twenty-eighth annual ACM symposium on Theory of computing* (1996), pp. 212–219.
- [38] C. Zalka, *Physical Review A* **60**, 2746 (1999).
- [39] M. Roget, S. Guillet, P. Arrighi, and G. Di Molfetta, *Physical Review Letters* **124**, 180501 (2020).
- [40] E. M. Stoudenmire and X. Waintal, *Phys. Rev. X* **14**, 041029 (2024), URL <https://link.aps.org/doi/10.1103/PhysRevX.14.041029>.
- [41] N. Shenvi, J. Kempe, and K. B. Whaley, *Physical Review A* **67**, 052307 (2003).
- [42] A. M. Childs and J. Goldstone, *Physical Review A* **70**, 022314 (2004).
- [43] A. Ambainis, A. Gilyén, S. Jeffery, and M. Kokainis, in *Proceedings of the 52nd Annual ACM SIGACT Symposium on Theory of Computing* (2020), pp. 412–424.
- [44] S. Apers, S. Chakraborty, L. Novo, and J. Roland, *Physical review letters* **129**, 160502 (2022).
- [45] J. D. Whitfield, C. A. Rodríguez-Rosario, and A. Aspuru-Guzik, *Physical Review A* **81** (2010), ISSN 1094-1622, URL <http://dx.doi.org/10.1103/PhysRevA.81.022323>.
- [46] C. Benjamin and N. Dudhe, *Journal of Statistical Mechanics: Theory and Experiment* **2024**, 013402 (2024).
- [47] I. Martínez-Martínez and E. Sánchez-Burillo, *Scientific reports* **6**, 23812 (2016).

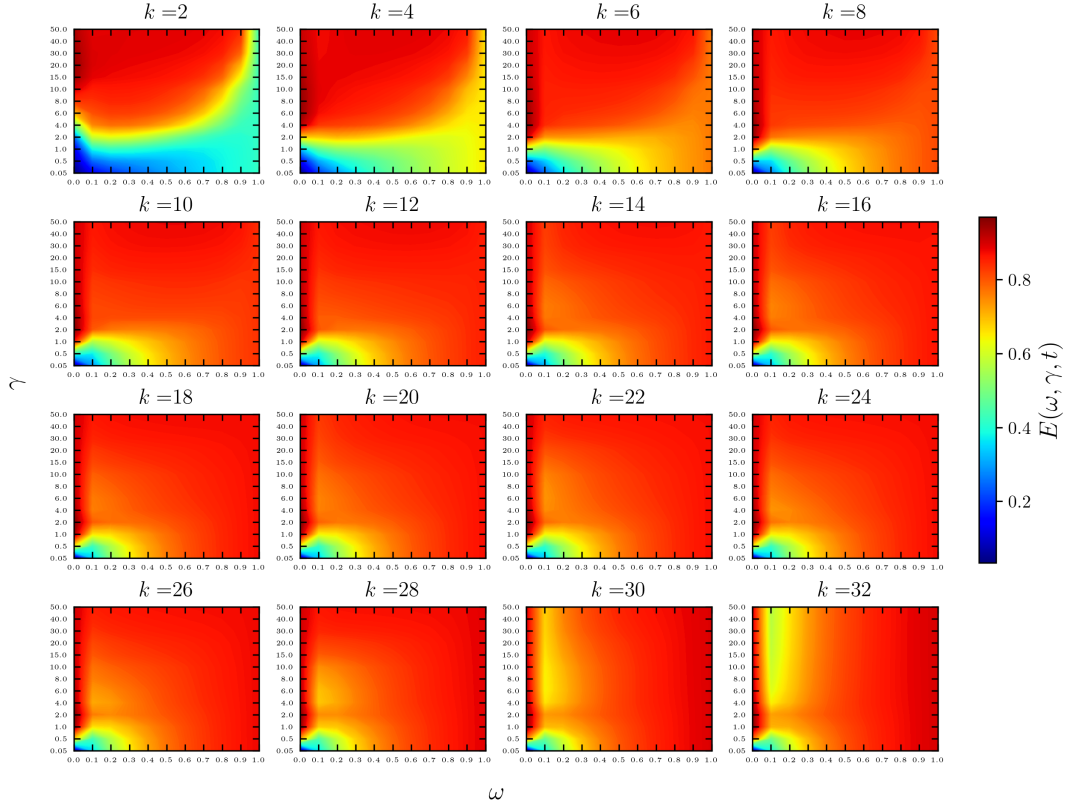


Figure 11: Stochastic Quantum Walk Search (SQWS) performances with different values of $\gamma \in [0.05, 50]$ on Ring-lattice graphs of size $N = 32$. The cycle graph graph is recovered for $k = 2$ and the complete graph for $k = 32$. An increase in the value of k corresponds to increasing the average connection of each vertex with its k -nearest neighbors. The time evolution is set to $t = 320$ units of time. The quantum walk dynamics is recovered for $\omega = 0$, the classical random walk for $\omega = 1$, and a linear combination of the two when $\omega \in]0, 1[$.

- [48] N. Dalla Pozza and F. Caruso, *Physics Letters A* **384**, 126195 (2020), ISSN 0375-9601, URL <http://dx.doi.org/10.1016/j.physleta.2019.126195>.
- [49] L.-J. Wang, J.-Y. Lin, and S. Wu, *Physical Review Research* **4**, 023058 (2022).
- [50] P. K. Schuhmacher, L. C. Govia, B. G. Taketani, and F. K. Wilhelm, *Europhysics Letters* **133**, 50003 (2021).
- [51] H. Tang, Z. Feng, Y.-H. Wang, P.-C. Lai, C.-Y. Wang, Z.-Y. Ye, C.-K. Wang, Z.-Y. Shi, T.-Y. Wang, Y. Chen, et al., *Physical Review Applied* **11**, 024020 (2019).
- [52] Z. Ding, X. Li, and L. Lin, *PRX Quantum* **5**, 020332 (2024).
- [53] F. Caruso, *New Journal of Physics* **16**, 055015 (2014), ISSN 1367-2630, URL <http://dx.doi.org/10.1088/1367-2630/16/5/055015>.
- [54] F. Caruso, A. Crespi, A. G. Ciriolo, F. Sciarrino, and R. Osellame, *Nature Communications* **7** (2016), ISSN 2041-1723, URL <http://dx.doi.org/10.1038/ncomms11682>.
- [55] N. D. Pozza, L. Buffoni, S. Martina, and F. Caruso, *Quantum reinforcement learning: the maze problem* (2021), 2108.04490.
- [56] L. Matsuoaka, H. Ohno, and E. Segawa, arXiv preprint arXiv:2411.12191 (2024).
- [57] A. W. Chin, A. Datta, F. Caruso, S. F. Huelga, and M. B. Plenio, *New Journal of Physics* **12**, 065002 (2010), ISSN 1367-2630, URL <http://dx.doi.org/10.1088/1367-2630/12/6/065002>.
- [58] F. Caruso, A. W. Chin, A. Datta, S. F. Huelga, and M. B. Plenio, *Phys. Rev. A* **81**, 062346 (2010), URL <https://link.aps.org/doi/10.1103/PhysRevA.81.062346>.
- [59] O. Mülken and A. Blumen, *Physics Reports* **502**, 37 (2011).
- [60] T. G. Wong, *Quantum Information and Computation* **22**, 53–85 (2022), ISSN 1533-7146, URL <http://dx.doi.org/10.26421/QIC22.1-2-4>.
- [61] S. Chakraborty, L. Novo, A. Ambainis, and Y. Omar, *Physical review letters* **116**, 100501 (2016).
- [62] S. Chakraborty, L. Novo, and J. Roland, *Physical Review A* **102**, 032214 (2020).
- [63] J. Malmi, M. A. Rossi, G. García-Pérez, and S. Maniscalco, *Physical review research* **4**, 043185 (2022).
- [64] D. Delahaye, S. Chaimatanan, and M. Mongeau, *Handbook of metaheuristics* pp. 1–35 (2019).
- [65] J. Johansson, P. Nation, and F. Nori, *Computer Physics Communications* **183**, 1760–1772 (2012), ISSN 0010-4655, URL <http://dx.doi.org/10.1016/j.cpc.2012.02.021>.

- [66] A. Hagberg, P. J. Swart, and D. A. Schult, Tech. Rep., Los Alamos National Laboratory (LANL), Los Alamos, NM (United States) (2008).
- [67] D. J. Watts and S. H. Strogatz, *nature* **393**, 440 (1998).